HIGH POWER OPERATION OF TWO SIDE-COUPLED STANDING WAVE LINAC STRUCTURES

by

J. McKeown, H.R. Schneider and S.O. Schriber
Atomic Energy of Canada Limited
Chalk River Nuclear Laboratories
Chalk River, Ontario, Canada

Introduction

The 805 MHz side coupler linear accelerator design developed at Los Alamos and operated successfully there at six per cent duty factor, has been tested to higher average powers at Chalk River Nuclear Laboratories. Two side coupled cavity tanks have been built and operated at power levels in excess of 50 kW at 100% duty factor. One of the tanks (Model 1) was built solely for investigating high power operation, while the other (Model 4) is a pre-accelerator section of a 4 MeV high intensity electron linac (1).

Tank Design and Construction

Model 1, shown in Fig. 1, consists of seven accelerating cells plus two half cell terminations. Segments for this tank were machined from Electron Prototype Accelerator forgings obtained from Los Alamos (2). The tank was brazed in two sections which were then joined with a flange connection and a knife edge seal. Twenty-four longitudinal cooling channels made by flattening $\frac{1}{2}$-inch diameter copper tubing, were soft-soldered to the wall of the tank. The side couplers were cooled by conduction from the segment only. Power was coupled in through an iris in the second accelerating cell from the end of the tank. The tank was pumped through the couplers on one side by an ion pump.

Model 4 is designed for an injection energy of 96 keV (β=.54) and an output of 1.37 MeV (β=.96). The large velocity change means that the cavity lengths must be increased to maintain synchronism. The accelerator cavity profile is shown in Fig. 2. Variation in cavity length is accomplished by adding straight sections of different lengths in the centre of the cell. The reason for this construction is historical. The copper segments used had originally been machined for a β=.65 tank. Fortunately, the cavity resonant frequency is quite insensitive to the length of extension, as can be seen from the graph of frequency versus cavity length in Fig. 3. Thus the design of a graded-β tank using these segments was relatively simple.

All the graphs in Fig. 3 pertain to the cavity profile in Fig. 2, and were obtained from field calculations using the numerical mesh program SAMINT-OPOPSCAN (3).

The design of the graded-β tank was generated by a cell by cell energy gain calculation for the synchronous particle, in a manner similar to that

TABLE 1

Model 4 Accelerating Cavity Design

Cavity No.	Cavity Length	Design Average Axial Field	Output Electron Energy	Power Dissipation Per Cell
	metres	MV/m	keV	kW
1	0.1147	1.20	196	2.30
2	0.1370	1.13	306	2.22
3	0.1505	1.09	420	2.15
4	0.1591	1.07	536	2.10
5	0.1649	1.05	654	2.05
6	0.1691	1.04	772	2.03
7	0.1721	1.03	892	2.00
8	0.1744	1.03	1012	1.98
9	0.1762	1.02	1131	1.98
10	0.1776	1.02	1252	1.96
11	0.1787	1.01	1373	1.95

used for design of Alvarez tanks.

Unequal accelerator cavity sizes combined with equal side coupler slot sizes lead to coupling factors and hence field amplitudes that vary from cell to cell. The magnitude of the field tilt was determined empirically from a simple three cell model, and taken into account in the design. Fig. 4 shows the axial field amplitude along the tank. The solid curve corresponds to the design while the plotted points were measured in the completed tank. Table 1 summarizes some of the design values for the accelerating cells of Model 4.

Fig. 5 is a photograph of the Model 4 tank prior to installation of shielding. The tank was built in two sections each about 1 meter long, and joined by a bridge coupler 80 cm long. Rf power is coupled to the tank through an iris in the bridge.

Attachment of the bridge to the accelerator sections was made by an edge-weld seal at the centre of the side couplers adjacent to the bridge as illustrated in Fig. 6. Also shown are the accelerator cavity cooling channels which differ from those of Model 1. In this case, prior to final assembly, two circumferential slots were machined into each segment and a cover brazed over them to form the cooling channels. Better thermal coupling to the region of maximum power dissipation is achieved in this way.

Tuning

Accelerating cell segments and coupling cavities were tuned prior to final brazing. The tuning was done in three steps; 1) segment tuning, 2) coupler tuning, 3) coupling constant adjustment.

In the case of Model 1, the segments were tuned by clamping them separately between copper plates in a pneumatic press. The resonant frequency of the two half cavities so formed was measured to determine the amount of copper to be removed from the drift tube nose. After two or three machining operations the cavity frequencies were brought within 100 kHz of the required tune value. For the purposes of this measurement the two half cavities were electrically isolated by metal plugs in the beam hole and a shorting plate in the coupling slot.

Couplers were tuned by a combination of machining copper from the capacitive loading bosses and adjusting the distance between the bosses with a specially designed jig. Their resonant frequencies were determined by clamping them in turn onto a segment in the tuning press and measuring the 0, $\pi/2$ and π-mode frequencies and then calculating the coupler frequencies using the usual coupled circuit model (4).

Coupling constants were checked after brazing of the couplers to the segments by measuring the two mode frequencies of a coupler and half cell with the other half cell of the segment detuned. Only small adjustments were necessary to equalize the coupling constants to within 1%.

The tuning of Model 4 while differing in detail followed the general procedure above. Because this tank is terminated in full cells however, it was necessary to tune these terminating cavities 1 MHz lower than the others to achieve minimum field in the side couplers.

After final brazing the Q values for Model 1 and Model 4 were 24,400 and 23,350 respectively. Both models showed a decrease in the $\pi/2$ mode frequency of approximately 0.5 MHz after brazing. Fitting of a Brillouin curve to the mode spectrum showed that second neighbour coupling had increased significantly. Possible origin of these changes are:

1) Sagging of the coupling slot during brazing
2) Cavity frequency shift because of improved rf contact at the braze joints
3) Braze alloy flow from the segment joint into the vicinity of the coupling slot.

Boroscope examination showed that such alloy flow did occur in some cells.

The Brillouin curve for Model 4 is shown in Fig. 7. The alternate high and low deviations of the measured frequencies from the fitted curve, near the ends of the curve, appear to be related to the break in periodicity caused by the bridge coupler. No such deviations were observed when the two tank sections were measured separately, but a similar behaviour has been noted in another bridge coupled tank, built for the Electron Test Accelerator.

Testing Facilities

Radiofrequency System

Two klystrons were used at various times in the high power tests of the structures viz, a 100 kW klystron (VA-853M) and a high efficiency 100 kW klystron (VA-3076). All were operated with the normal service interlocks for vacuum and water flow. A fast protect system was used to detect and annunciate excessive forward or reverse power transients, rf arcs at the klystron window and excessive body current. These signals remove the drive power to the klystron in less than 1 μsec. If the alarm condition persists for longer than 30 μsec a crowbar system is triggered to remove the dc voltage from the tube. Rf arcs at the klystron window or excessive body current produce an unconditional crowbar.

The low power drive system consists of a voltage-programmable stable oscillator, fixed attenuator, isolator, diode switch and directional coupler feeding 10 mW of rf power to a transistorized 30 db class C amplifier. The klystrons are generally run unsaturated and the drive power of 0-10 watts is provided through a voltage programmable PIN modulator.

The klystrons were commissioned by dumping the power into a flat water load. Calorimetric measurements of efficiency were taken and with careful tuning at 805 MHz, efficiencies of 53% for the VA-853M and 65% for the VA-3076 were achieved at 100 kW. It was found however that the klystrons behaved more stably although at lowered efficiency when tuned at broader bandwidths of around 7 MHz.

Driving into resonant loads at high power imposes considerable demands on the rf control systems. Our approach to the solution of some of these problems are more fully discussed elsewhere (1). In the experiments discussed here a high power isolator having an insertion loss of 0.3 db and reverse attenuation of 3.8 db was used to provide some tolerance to excursions from resonance. Our reverse power trip was set at 2 kW by a signal taken from a WR-975 waveguide directional coupler protecting the klystron.

Tank Resonance Control

It was initially planned to provide resonance control of Model 1 through its cooling water temperature. This proved unsuccessful. We decided therefore to experiment with control of the tank resonant frequency using a mechanical tuner in the bridge of Model 4 for fast control while the cooling system regulates the water temperature to provide slow resonance control only. Experiments have been performed with Model 4 to keep the frequency fixed by using the bridge tuning plunger to compensate for thermal changes at high power. Results of these experiments are presented elsewhere.

All high power tests described below were performed with a constant inlet water temperature. The klystron drive frequency was controlled by an automatic frequency controller which adjusted the frequency of the master oscillator to the resonant frequency of the tank. The controller operates by frequency modulating the drive frequency with a 10 kHz signal, giving a maximum frequency deviation of 1.5 kHz, and then detecting the resulting amplitude modulation of the cavity fields with a crystal detector. The demodulated cavity signal and the 10 kHz modulating signal are combined in a phase sensitive detector circuit to produce the feedback control signal.

Structure Properties at High Power

Tank Commissioning

For the Model 1 tests an arc detector was used to trip the klystron power in addition to the vacuum, radiation and cooling water flow trips used by Model 4. Initial attempts to run the tanks by gradually increasing the cw power led to numerous klystron trips from arcs, reverse power and poor vacuum. The latter was presumably due to multipactoring. Even after the tanks have been run at high cw power for long periods a recommissioning procedure is required before the structures will support again the design fields of 1 MV/m.

A satisfactory conditioning procedure was developed as follows. At very low average power the tank is pulsed to high peak power for approximately 20 μsec at a fixed resonant frequency. An RC filter is set at 30 μsec so that the reverse power peaks at the beginning and end of the pulse do not activate the reverse power trips. Usually the tank pressure increases from a base level of around 10^{-7} torr to 10^{-6} torr during this cleaning process. When the tank vacuum improves the pulse width

is increased until the average power ceases to become negligible, resulting in a change of the tank resonant frequency. At this point the rise and fall time of the pulse fed to the PIN modulator in the klystron drive line is increased to a few milliseconds. This operation usually gives rise to multipactor resonances which again increase the tank pressure. After some hours the frequency of multipactoring decreases and when it disappears the base pressure is regained. At this point cw operation can begin. Recently an isolator providing 17.5 db of reverse power attenuation, when the ferrites are cold, has been installed. The ability to withstand larger arc induced impedance mismatches at low duty factors will allow more rapid tank conditioning in the future.

Temperature Distributions

Structure de-tuning will occur through thermal expansion of the structure. Of particular interest is the temperature distribution in the septum between two accelerating cells. A numerical calculation (5) of the temperature gradient in the Model 1 cavities was compared with measurements taken at two different penetrations of two cells when a net power of 20 kW (2.5 kW/cell) was supplied to the structure. The depths and temperatures shown in Table 2 are measured relative to the outer surface.

TABLE 2: Septum Temperatures in Model 1

Penetration into Septum (cms)	Mesh Calculation (^{o}C)	Measured	
		Cell #1	Cell #7
8.3	22.2	17.5^{o}C	16.5^{o}C
5.7	7.8	5^{o}C	5.2^{o}C

Copper temperature distributions relative to the average cooling water temperature were measured for the design powers of 20 kW (2.5 kW/cell) and 32 kW (2.57/cell average) for Model 1 and Model 4 respectively. The data presented in Fig. 8 show the copper temperatures relative to the inlet cooling water temperature.

Rf Performance at High Power

(i) Frequency changes

Frequency increases attributed to the change in the dielectric constant with removal of dry nitrogen from the tanks were found to be 222 kHz and 201 kHz for Model 1 and Model 4 respectively. This is consistent with a calculated value of 219.8 kHz for Model 1. Measurements were also made of the frequency changes at zero power resulting from changes in the average temperature. The thermal sensitivity of the $\pi/2$ mode frequency was found to be -13.6 kHz/^{o}C consistent with the thermal expansion of copper.

The physical distortion of the cell profile at high power decreases the $\pi/2$ mode frequency. This decrease is due primarily to the expansion at the high electric field point of the accelerating cell nose. For both tanks the frequency decreases almost linearly with power as shown in Fig. 9. In Model 1 the drop in frequency is constant at 158 kHz/kW/cell. Of this, 68 kHz/kW/cell comes from the increase in the ambient temperature of the walls and the remaining 90 kHz/kW/cell is assumed to come from profile distortion. In Model 4 the total drop in frequency from both sources has an average value of 87 kHz/kW/cell. The considerable decrease in sensitivity of the latter tank to thermal changes caused by rf power, demonstrates the superior heat transfer characteristics obtained by machining the cooling channels into the tank structure.

Field Distributions

The Model 1 tank was coupled to give a low power VSWR of 1.04. The match changes smoothly from a slightly undercoupled condition to a slightly overcoupled condition with increase in power. In Model 4 an overcoupled match of 1.15 was achieved through a circular iris in the bridge of 9.65 cms in diameter. There is some structure in the reverse power curve in going from low to high power at 100% duty factor. This may be due to small discharges which do not seem to occur when the klystron is pulsed at very low average power.

Fig. 10 shows the variation of field tilt with tank power for Model 4. The results have been normalised to

consider only the ratio of signals from the field probes located at the opposite ends of the tank sections and the complete tank. The rms deviation from the mean field ratio is 2.4% for these data without evidence of any systematic trend.

A more sensitive measure of the tank behaviour is found from the side-coupler fields. A comparison of side coupler fields measured for both cw and pulsed operation with a peak input power of 61.5 kW in Model 1 and 32 kW in Model 4 showed wide variations. The results are given in Table 3. These can only be accounted for by changes in the cell-to-cell coupling and small changes in relative cell resonant frequencies due to temperature differences. Model 4 does not show quite as large a spread as does Model 1.

Resonant frequencies of modes other than the $\pi/2$ mode were measured at various $\pi/2$ mode power levels. Power for these modes was obtained by driving one side coupler with a swept signal of 10 watts and detecting in another coupler using a notch filter to suppress the $\pi/2$ mode. A marker frequency from a stable oscillator was imposed on the swept frequency in order to measure accurately the mode frequencies. The results of an analysis of the mode frequencies using the coupled circuit analog are shown in Table 4.

For both tanks the model shows the expected trend of a decrease in resonant frequency for both accelerating cells and side couplers. The first and second neighbour coupling is independent of power

TABLE 3: Ratio of High Power cw/Pulsed Side Coupler Fields

	Model 1	Model 4
	61.5 kW 10% duty factor 0.3 ms pulse	34 kW 1.2% duty factor 3 ms pulse
Coupler Number	cw field/pulsed field	cw field/pulsed field
1	1.55	1.14
2	0.25	0.66
3	1.57	0.57
4	1.41	0.82
5	1.44	0.93
6	2.49	1.3
7	0.70	1.3
8	1.02	0.96
9		0.83
10		1.07
11		1.2

TABLE 4: Results from Mode Spectra Fit at Different Power Levels

$\pi/2$ Mode Input Power (kW)	Accelerating Cell Frequency (MHz)	Side Coupler Cell Frequency (MHz)	Nearest Neighbour Coupling Constant	Second Nearest Neighbour Coupling Constant	Stop Band (MHz)
		Model 1			
0	803.994	802.205	0.04456	-0.00395	0.207
2.5	803.951	802.164	0.04456	-0.00392	0.215
3	803.902	802.117	0.04456	-0.00394	0.208
15	803.720	801.889	0.04457	-0.00394	0.254
20	803.588	801.766	0.04458	-0.00395	0.239
		Model 4			
0	806.878	804.841	0.04503	-0.00484	0.093
5	806.841	804.787	0.04507	-0.00483	0.112
15	806.802	804.681	0.04496	-0.00490	0.152
25	806.686	804.561	0.04507	-0.00480	0.197
32	806.619	804.488	0.04506	-0.00474	0.225

for Model 1. For Model 4 the second neighbour coupling peaks slightly at intermediate powers but the results are not conclusive. For both tanks the stop band increases with power, significantly for Model 4.

The results for both tanks are surprising as one would expect the accelerating cell frequencies to change at a greater rate than the side couplers with changes in power. The coupled circuit analysis will provide a better analog to structure behaviour for the Model 1 tank than the Model 4 tank. For the latter tank the model provides only an average of the coupling constants. Also the bridge in Model 4 with its consequent lack of second neighbour coupling and the full end cells disturbs the symmetry of the model. It is nevertheless somewhat surprising that the model indicates larger coupler frequency shifts than accelerating cell frequency shifts at high power for both tanks.

The phase differences between first and last cells was less than 0.7° from zero power to 20 kW for Model 1. From coupled loop model calculations these differences would imply less than ± 1.5% changes in relative axial field changes. The phase changes for Model 4 were greater but a clearly defined systematic trend was observed. When the power was increased from a calorimetrically measured power of 6 kW to 39 kW the low energy end of the structure decreased in phase by 1.3° relative to the high energy end of the structure.

Model 4 Beam Test

In a preliminary run a beam of 250 μA was accelerated through Model 4 and stopped in a copper Faraday cup immediately after the final cell. The average beam energy was determined from radiation and calorimetric measurements to be (1.24 ± 0.1 MeV) for a net power of 24.1 kW. The deduced value for the effective shunt impedance (ZT^2), assuming a synchronous phase angle of 26°, is 67.7 ± 8 MΩ, or 24% below the value of 88.3 MΩ calculated for the case with couplers and coupling slots neglected.

Conclusion

The side coupled linear accelerator design developed at Los Alamos has been tested up to axial fields of 1.6 MV/m with 100% duty factor. The structures are stable at these power levels and have been used to accelerate a test electron beam to 1.34 MeV at average axial fields of 1.1 MV/m. Under these conditions the axial electric field tilts are less than 2.4% and the phase changes were found to differ by 1.3° from low power measurements.

Milling the cooling channels into the segment structure reduces detuning at high power. Lack of water cooling in the side couplers is a weakness in the present designs and coupler cooling channels should be incorporated in future tanks to be used at high power.

Acknowledgements

We are indebted to S.B. Hodge who was responsible for the mechanical design of the tanks.

References

(1) "The Chalk River Electron Test Accelerator" J.S. Fraser, S.H. Kidner J. McKeown and G.E. McMichael, paper this conference.

(2) "Design and Initial Performance of a 20 MeV High Current Side Coupled Cavity Electron Accelerator" E.A. Knapp and W.J. Shlaer, Proceedings of 1968 Proton Linear Accelerator Conference (BNL 50120) p. 635.

(3) O. Aboul-Atta and A. Malecki, private communication.

(4) "Standing Wave High Energy Accelerator Structures" E.A. Knapp, B.C. Knapp, and J.M. Potter, Review of Scientific Instruments 39, 979, (1968).

(5) CAVE, a program to calculate temperature distributions in linac cavities, J. Griffiths, private communication.

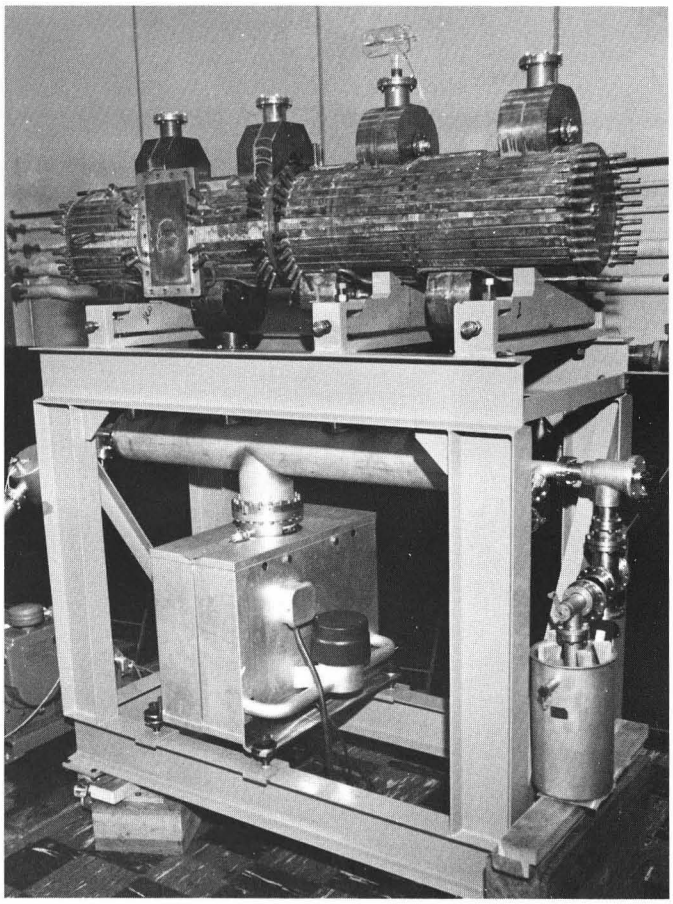

Figure 1. Photograph of Model 1

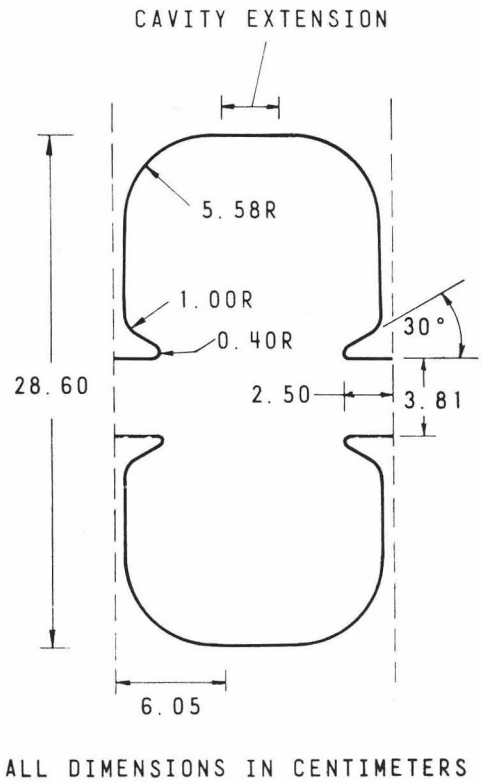

Figure 2. Model 4 Cavity Profile

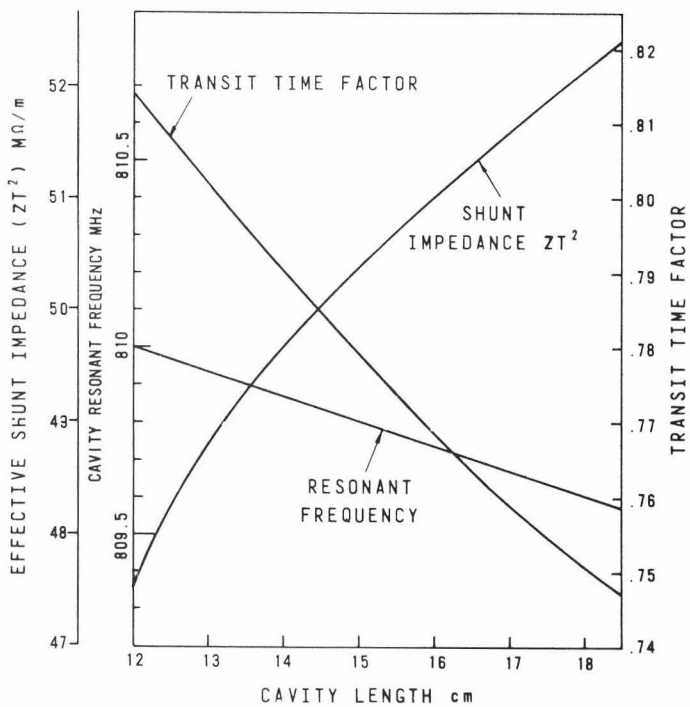

RESULTS OF MESH CALCULATIONS FOR MODEL 4 ACCELERATING CAVITIES

Figure 3. Results of Mesh Calculations for Model 4 Accelerating Cavities

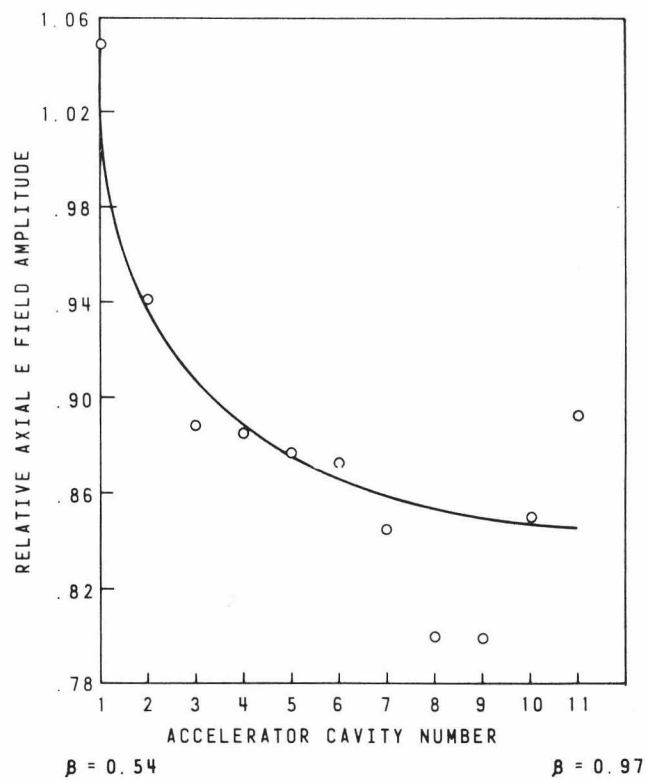

Figure 4. Model 4 Axial Electric Field

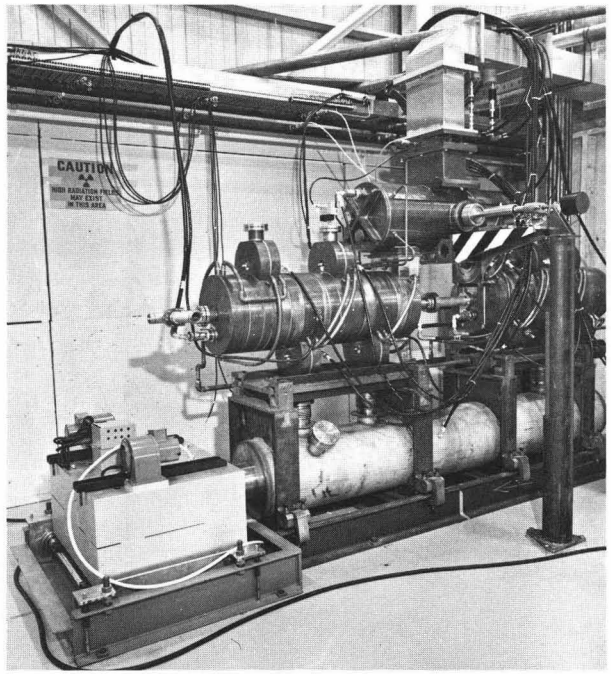

Figure 5. Photograph of Model 4

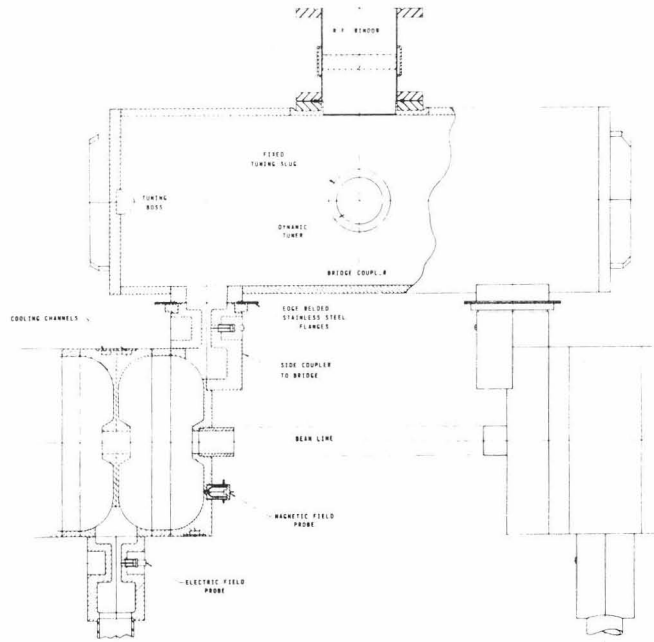

Figure 6. Bridge Coupler Design and Segment Cooling Channels

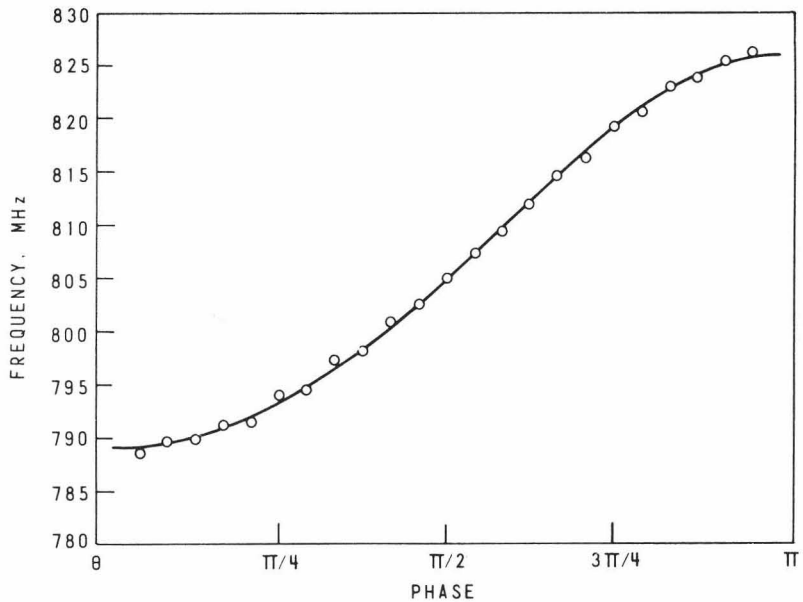

Figure 7. Brillouin Curve for Model 4

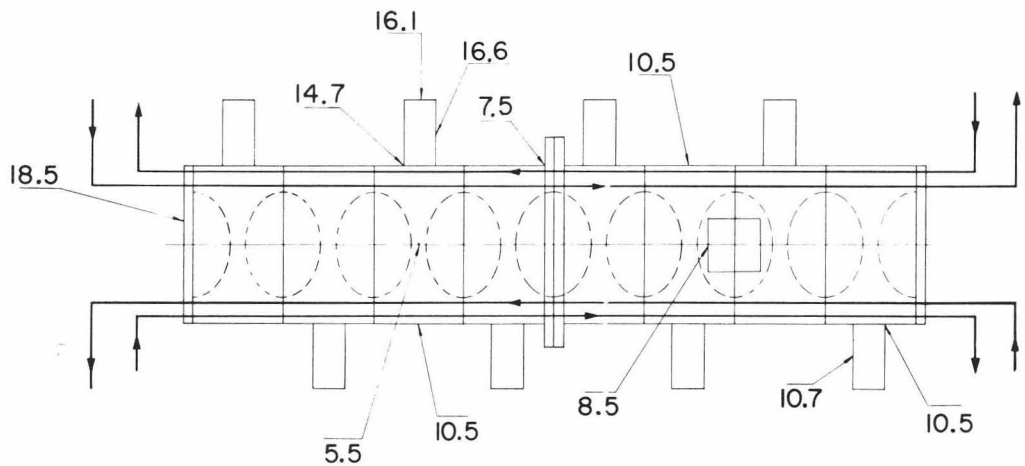

Figure 8. Temperature Distributions in Model 1 and Model 4 at Design Power. The numbers refer to temperatures in °C above the inlet water temperature.

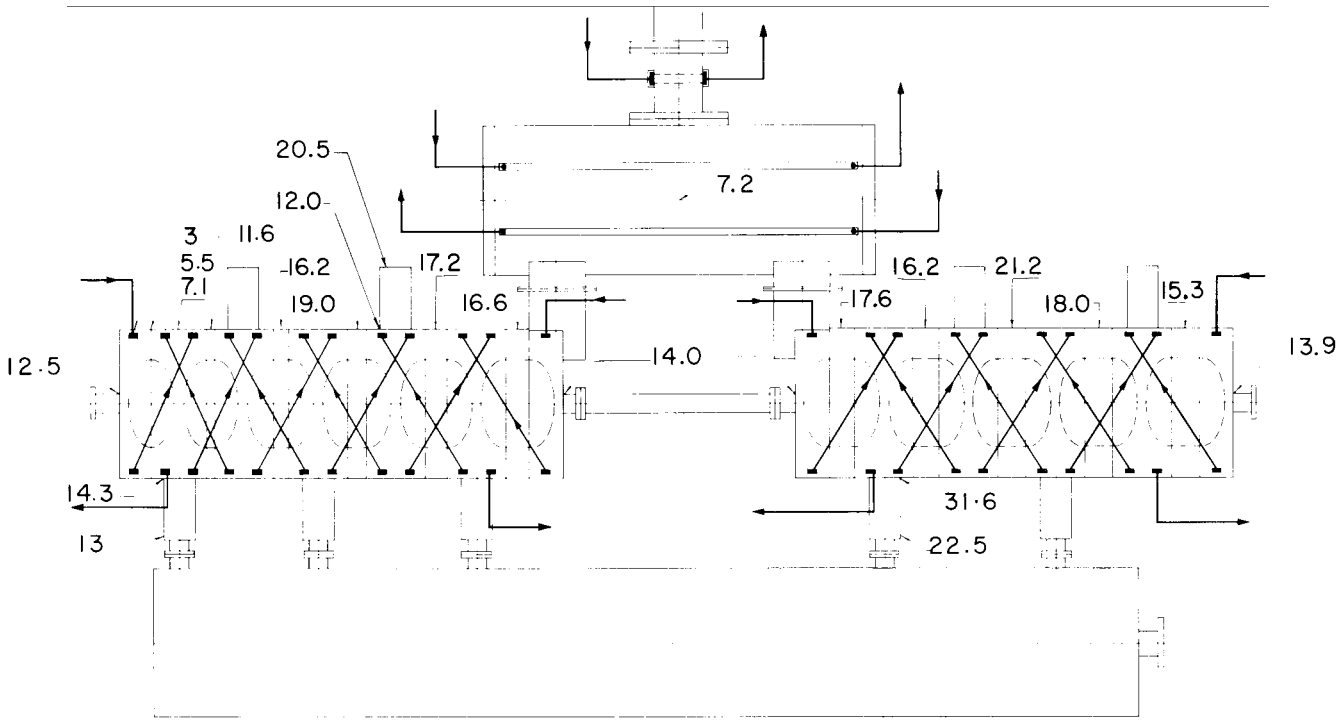

Figure 8b

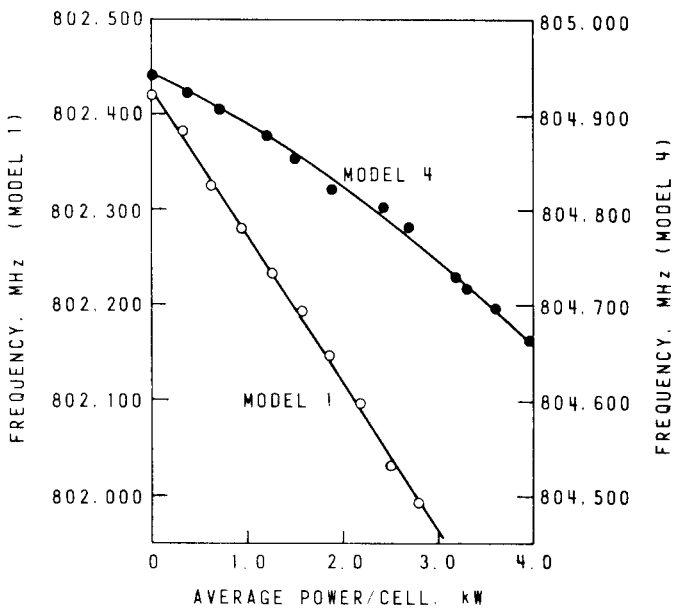

Figure 9. π/2 Mode Frequency as a Function of Power

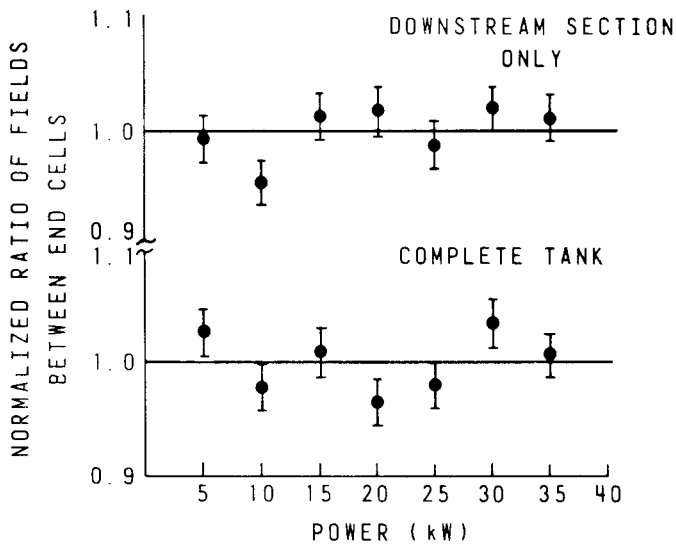

Figure 10. Variation of Field Tilt with Tank Power for Model 4